International Journal of Bioprinting

RESEARCH ARTICLE

3D-printed dual drug delivery nanoparticle-loaded hydrogels to combat antibiotic-resistant bacteria

David Martínez-Pérez[1†], Clara Guarch-Pérez[2†], Muhammad Abiyyu Kenichi Purbayanto[1], Emilia Choińska[1], Martijn Riool[2], Sebastian A. J. Zaat[2], Wojciech Święszkowski[1*]

[1]Faculty of Materials Science and Engineering, Warsaw University of Technology, Wołoska 141, 02-507, Warsaw, Poland

[2]Department of Medical Microbiology and Infection Prevention, Amsterdam Institute for Infection and Immunity, Amsterdam UMC, University of Amsterdam, Meibergdreef 9, 1105 AZ, Amsterdam, the Netherlands

Abstract

Implant-associated infections are not easy to diagnose and very difficult to treat, due to the ability of major pathogens, such as *Staphylococcus aureus,* to develop biofilms and escape the immune response and antibiotic treatment. We, therefore, aimed to develop a 3D-printed dual rifampicin (Rif)- and vancomycin (Van)-loaded polylactic-co-glycolic acid (PLGA) nanoparticles (NPs) delivery system based on hydrogels made of gelatin methacrylate (GelMA). The release of Rif and Van from NPs manufactured from different PLGA molecular weights was studied in phosphate-buffered saline for 21 days. Low molecular weight PLGA NPs exhibited the fastest release of Rif and Van within the first 7 days and were selected for antimicrobial evaluation. Four different GelMA-based 3D-printed samples were successfully produced, carrying non-loaded NPs, Rif-NPs, Van-NPs, or alternating layers of Rif-NPs and Van-NP. The exposition of *S. aureus* against increased concentrations of Rif or Van produced new resistant strains to Rif (Rif^R) or Van (Van^R). The GelMA hydrogel co-delivering Rif and Van eradicated *S. aureus* RN4220 Rif^R and RN4220 Van^R strains. *S. aureus* RN4220 and *S. aureus* AMC 201 colonies developed resistance to Rif after contact with the GelMA hydrogel containing only Rif-NPs which appeared to be due to known mutations in the *rpoB* gene. In conclusion, 3D-printed GelMA hydrogel loaded with PLGA Rif-Van-NPs drug delivery system show promising *in vitro* results to prevent implant-associated infections caused by antimicrobial-resistant bacteria.

Keywords: 3D printing; Antibiotic resistance; *Staphylococcus aureus*; Controlled drug delivery; Gelatin methacrylate; Nanoparticles

†These authors contributed equally to this work.

***Corresponding author:**
Wojciech Święszkowski
(wojciech.swieszkowski@pw.edu.pl)

Citation: Martínez-Pérez D, Guarch-Pérez C, Purbayanto MAK, *et al*., 2023, 3D-printed dual drug delivery nanoparticle-loaded hydrogels to combat antibiotic-resistant bacteria. *Int J Bioprint,* 9(3): 683.
https://doi.org/10.18063/ijb.683

Received: October 04, 2022
Accepted: November 08, 2022
Published Online: February 13, 2023

1. Introduction

Implant-associated infection is a devastating healthcare complication worldwide. The infection rates in patients with total arthroplasties for the hip and knee are 0.5%–1% and 1%–4%, respectively. Infection rates from closed fractures with fracture fixation

devices range from 5% to 10%, and open fractures with these devices show even higher rates up to 30%[1]. The majority of infections caused by orthopedic devices are brought on by opportunistic pathogens and bacteria found in the skin microbiota[2]. The biofilm-forming species *Staphylococcus aureus* and *Staphylococcus epidermidis* are the most common pathogens related to implant-associated infections[2-4]. *Staphylococci* can attach to and colonize the implant surface and surrounding tissue forming a biofilm structure, thereby becoming less susceptible to antibiotics and immune defenses because the antibiotics and immune defenses cannot correctly penetrate the biofilm and target the bacteria[2,5].

Clinically, implant infections are mainly prevented by the application of skin antiseptics, such as iodine povidone or chlorhexidine, and systemic antibiotic prophylaxis, such as intravenous administration of cefazolin 30 to 60 min before the surgical procedure[1]. Despite the reduction of infection rates, systemic antibiotic prophylaxis and antiseptics cannot provide sufficient protection on the surgical wound in all cases. When compared to systemic administration, local antibiotic prophylaxis provides a higher local antibiotic concentration and bioavailability, at the bone site, with minimum toxicity effects[6,7].

Poly (methyl methacrylate) (PMMA), also known as bone cement, is one of the most typical biomaterials applied in orthopedics as a local antibiotic delivery system[1]. The surgeon usually mixes the PMMA powder with antibiotics, such as gentamicin sulfate, tobramycin, or vancomycin (Van), to obtain a paste. Then, the surgeon applies the paste as a coating of bone or joint implantable devices, or as a spacer in infection treatment revision surgery. However, bone cement is not biodegradable, shows poor antibiotic release profiles, and can only be combined with a limited number of antimicrobial compounds[8]. In many cases, only a single antibiotic is used for local delivery, and in view of the poor release profile of the antibiotic, an increased risk of resistance development is inevitable. For example, the exposure of *S. aureus* or *Pseudomonas aeruginosa* to antibiotics such as rifampicin (Rif) or ciprofloxacin is related to a high risk of resistance development[9,10]. For that reason, it is not advisable to administer Rif as a monotherapy. A combination of antibiotics incorporated in the biomaterial will reduce the risk of selection of resistant bacteria to one antibiotic and will thereby eradicate the infection. For example, Rif is an essential antibiotic used in combination with other antibiotics such as Van, or with both Van and gentamicin sulfate, for the treatment of bacterial biofilm bone implant infection attributed to its ability to penetrate and destroy the bacterial biofilm[11]. Unfortunately, Rif cannot be used in bone cement since it acts as a free radical neutralizer and negatively affects the polymerization process of the cement[12]. Therefore, alternative biomaterials incorporating Rif and other antibiotics have been investigated. Darouiche *et al.* described the *in vivo* local efficacy of a combination of minocycline with Rif sprayed onto titanium pins as a prophylactic implant coating[13]. Later, Inzana *et al.* developed a 3D-printed biomaterial system with a dual antibiotic delivery system of Rif and Van to treat an established bone biofilm infection[14].

Furthermore, Sanz-Ruiz *et al.* developed a system with Rif microcapsules of alginate that can be incorporated into bone cement in combination with other antibiotics[15]. However, these solutions have some limitations, such as limited control over the release profile of the drug and not suitable for 3D bioprinting (3D printing of living cells) in bone regeneration therapies. Furthermore, 3D printing technology allows personalized geometries specifically for the necessity of the patient[16]. Additive manufacturing (AM) technology, also known as 3D printing, increases the possibility for creating orthopedic devices with more combinations of biomaterials and antimicrobial compounds with a controlled drug release profile.

The existing standard for 3D printing in biomedical research is the "ISO/ASTM 52900 Standard Terminology for Additive Manufacturing – General Principles – Terminology"[17]. This standard defines the seven standard 3D printing types: binder jetting[18,19], direct energy deposition[20], material extrusion (mechanical and pneumatic)[21,22], material jetting (inkjet, microvalve, laser-assisted, acoustic, and PolyJet)[23,24], powder bed fusion (selective laser sintering, selective laser melting, direct metal printing, and electron beam melting)[25], sheet lamination (laminated object manufacturing)[26], and vat photopolymerization (stereolithography apparatus and direct light processing)[27,28]. In this work, the material extrusion (pneumatic) technology was selected for its ability to create softer biomaterials, like hydrogels, that can be applied in bone regeneration[29], especially in joints, or as a coating on orthopedic implants[30].

Hydrogels have been deeply investigated for their application in bone tissue engineering because of their porosity, degradation properties, and high-water content[31,32]. In recent years, gelatin methacrylate (GelMA) hydrogels have been studied in tissue engineering for bone regeneration applications because of their high biocompatibility and the possibility of being photochemically crosslinked, which enable the formation of a stable gel at physiological temperature[33]. In addition, GelMA hydrogels have promising bioink characteristics for 3D printing, which is necessary to create scaffolds with different porosities and geometries to incorporate cells or

compounds such as growth factors or antimicrobial agents. PLGA (lactic-*co*-glycolic acid) is a polymer used extensively for drug delivery formulations and is approved by the U.S. Food and Drug Administration (FDA)[34]. Previous works studied PLGA nanoparticles (NPs) encapsulating different antimicrobial compounds and their effectivity in preventing or treating bacterial infections[35,36].

Therefore, this study aimed to develop a 3D-printed GelMA-PLGA NPs multilayer structure that allows local and sustained delivery of two antibiotics, i.e., Rif and Van, to prevent the selection of antibiotic-resistant bacterial strains and allow the eradication of even the antibiotic-resistant strains. The formulation developed in this work may be applied mainly as a 3D-printed coating on orthopedic implants or as a bioink for tissue engineering solutions. This technique may offer a personalized therapy based on the patient's needs where the physician will have the option to combine (a wide range of) different antibiotic inks with a personalized drug loading and controlled release.

2. Materials and methods

2.1. Materials

Type A gelatin from porcine skin (G1890), methacrylic anhydride (94%), 2-Hydroxy-4-(2-hydroxyethoxy)-2-methylpropiophenone (Irgacure 2959, 98%), O-Phthaldialdehyde (OPA), butylamine, Span 80, rifampicin (Rif), vancomycin (Van), and sodium borate were ordered from Sigma-Aldrich (St. Louis, MO, United States. Poly (D,L-lactide-*co*-glycolide) (PLGA; acid endcap) low (LMW; AP081) and medium (MMW; AP041) molecular weight was purchased from Akina, Inc. (West Lafayette, IN, United States) and high molecular weight (HMW) Purasorb PDLG 5004A was purchased from Corbion (Amsterdam, the Netherlands). Phosphate-buffered saline (PBS) tablets were purchased from Carl Roth Gmbh (Karlsruhe, Germany). Polyvinyl alcohol (PVA) 87%–89% hydrolyzed 13–23 kDa was purchased from Acros Organics (Geel, Belgium). Sorbitan Monooleate (Span 80) was purchased from Glentham Life Science (Corsham, United Kingdom). Dichloromethane (DCM) was purchased from Stanlab (Lublin, Poland).

2.2. Synthesis of GelMA

GelMA was synthesized as previously described[33]. In short, type A porcine gelatin was dissolved at 10% (w/v) in PBS at 60°C. About 0.8 mL of methacrylic anhydride per gram of gelatin was added dropwise under constant stirring (Figure 1a). After 3 h, the solution was dialyzed against deionized water at 37°C for 5 days to remove the methacrylic acid and anhydride. The solution was freeze-dried for 72 h and stored at -20°C until further use.

The degree of functionalization (DoF) was determined as previously described[33]. OPA reacts in the presence of primary amine or thiol groups to generate a fluorescent product. The OPA reagent was prepared by dissolving 2.5 g of OPA in 560 mL of sodium borate 40 mM (pH 10.4), 65.5 mL of methanol, and 3 mL of 2-mercaptoethanol. Gelatin or GelMA were dissolved at 1% (w/v) in deionized water, mixed with OPA reagent in a volume ratio 1:2 (sample:OPA), and fluorescence was measured at 340/455 nm (microplate reader Fluostar Omega, BMG Labtech, Jozefow, Poland). Butylamine was used as a standard for the calibration curve (**Figure S1**). The DoF was calculated according to the following equation:

$$DoF = \frac{free\ amine\ mol\ gelatin - free\ amine\ mol\ GelMA}{free\ amine\ mol\ gelatin\ solution} \quad (I)$$

2.3. Preparation of Rif-PLGA nanoparticles

NPs loaded with Rif (Rif-NPs) were synthesized following the single emulsion and evaporation process, as previously described[37] (Figure 1b.1). PLGA with three different molecular weights (LMW, MMW, and HMW) was used. First, 500 mg of PLGA were dissolved in 20 mL of DCM. Rif was dissolved in the solution at 15% (w/w). The solution was poured into 200 mL of PVA 2% (w/v) and sonicated for 1 min at 40% amplitude. The solution was left under stirring overnight to allow evaporation of DCM. The obtained Rif-NPs were washed with deionized water by centrifugation at 6,000 rpm for 30 min. The washing process was repeated three times. The supernatants were stored for further analysis, and the washed Rif-NPs were freeze-dried and sterilized by gamma radiation (25 kGy dose). Rif-NPs were stored at 4°C for further use.

2.4. Preparation of Van-PLGA nanoparticles

NPs loaded with Van (Van-NPs) were synthesized by the double emulsion and evaporation process, as described previously[38] (Figure 1b.2). Van-NPs with three different molecular weight PLGA polymers were synthesized, i.e., with LMW, MMW, and HMW. First, 500 mg of PLGA were dissolved in 20 mL of DCM. Then, Span80 was added to the solution at 1% (w/v). Two milliliter of Van at 4.5% (w/v) in PBS were added to the solution and sonicated for 1 min and 40% amplitude (Vibra-cell, Sonics & Materials Inc., Newton, CT, United States). The emulsion was poured into 200 mL PVA 2% solution and sonicated at 40% amplitude for 1 min. The evaporation, cleaning, freeze-drying, and sterilization processes were performed as described above for the Rif-NPs. Non-loaded NPs (C-NPs) were prepared by following the same method as Van-NPs, but without Van in the PBS.

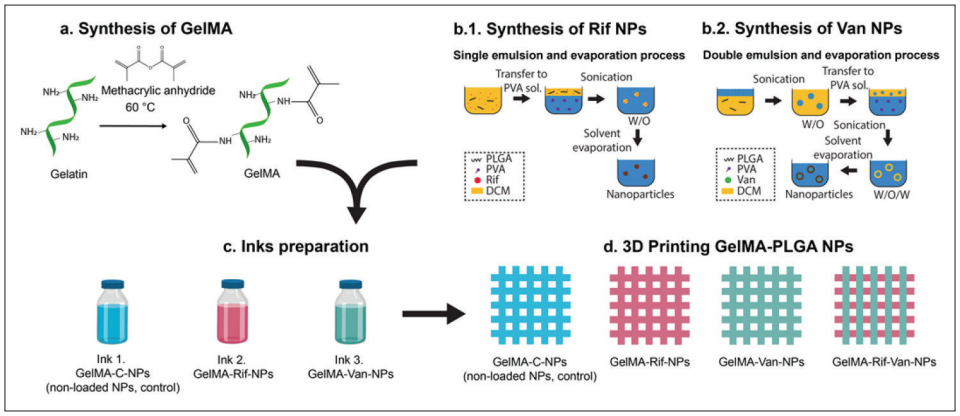

Figure 1. (a) Synthesis of GelMA by methacrylic anhydride reaction. (b.1) Synthesis of PLGA Rif-NPs by double emulsion and evaporation process and (b.2) synthesis of PLGA Van-NPs by single emulsion and evaporation process. (c) Combination of GelMA and PLGA NPs to prepare the inks: GelMA-C-NPs (non-loaded NPs; control), GelMA-Van-NPs, and GelMA-Rif-NPs. (d) 3D Printing of GelMA hydrogels containing C-NPs, Rif-NPs, Van-NPs, and combination of Rif-NPs and Van-NPs (in separate layers).

2.5. Characterization of PLGA nanoparticles

Scanning electron microscopy (SEM; SU8000, Hitachi, Tokyo, Japan) was used to study the size distribution of PLGA NPs. Histograms (n = 250) were performed to determine the mean size and polydispersity index (PDI) (Equation II) using ImageJ software. The amount of Rif or Van entrapped in the NPs was determined by indirect quantification of the free drug in the supernatant obtained in the cleaning process (see above), Van quantification was performed using the OPA reaction (see above) and fluorescence was measured at 340/455 nm after 15 min at room temperature. Rif quantification was performed by directly measuring absorption at 335 nm. PDI, encapsulation efficiency (EE), and drug loading (DL) were determined by the following equations:

$$PDI = \left(\frac{\sigma}{d}\right)^2 \quad \text{(II)}$$

$$EE = \frac{Total\ amount\ of\ drug - Amount\ of\ drug\ in\ supernatant}{Total\ amount\ of\ drug} \quad \text{(III)}$$

$$DL = \frac{Total\ amount\ of\ drug - Amount\ of\ drug\ in\ supernatant}{Amount\ of\ polymer} \quad \text{(IV)}$$

Where σ is the standard deviation, and d is the mean size of the NPs.

2.6. *In vitro* drug release

Release of antibiotics from PLGA NPs was determined after dispersing 30–50 mg of freeze-dried NPs in 1 mL of PBS (pH 7.4) at 37°C under shaking at 60 rpm. At fixed time points, samples were centrifuged (NPs forming a pellet), and all the supernatant was taken and replaced with fresh PBS. Then, the NPs were redispersed using a vortex. The concentration of Rif and Van in the supernatant was determined as described above.

2.7. Preparation of GelMA-PLGA NPs inks

A solution of GelMA 10% (w/v) was prepared in deionized water at 40°C. A photoinitiator (Irgacure 2959) was added to the solution to a final concentration of 0.05% (w/v). The solution was sterilized using a polystyrene syringe filter (0.22 μm). Three different inks were prepared (GelMA C-NPs [non-loaded; control], Rif-NPs, and Van-NPs) (Figure 1c) by dispersing sterile LMW PLGA NPs in sterile water and sonicating in an ice bath for 5 min, followed by adding them to the GelMA solution. The final concentrations of GelMA and PLGA NPs were 7.5% (w/v) and 30% (w/w), respectively.

2.8. Rheological and mechanical characterization

A dynamic shear rheometer (Ares, TA Instruments, New Castle, DE, United States) was used to study the physical crosslinking of GelMA and GelMA-NPs hydrogels within a range of temperatures from 5°C to 40°C. These studies were performed using cone plates of 50 mm diameter, 50.8 mm gap, 1 Hz, and 10% of strain. Mechanical properties of GelMA and GelMA-NPs hydrogels were studied using a DMA (Dynamic Mechanical Analysis Q800, TA Instruments, New Castle, DE, United States). Samples were prepared by pouring hydrogel solution on a polymethylsiloxane (PDMS) mold (cylindrical shape, 6.5 mm diameter, and 9 mm height) and exposure to 25 mW/cm^2 UV light (BlueWave 75 UV Light Curing Spot Lamp, 365 nm, Torrington, CT, United States) for 90 s. The elastic modulus was determined in the linear region of stress–strain of compression tests (5%–20% strain region) using the DMA Q800.

2.9. 3D printing of GelMA-PLGA NPs hydrogels

The inks were transferred to a 30-mL sterile syringe and kept in the cartridge (3D Bioplotter, Envisiontec GmbH, Gladbeck, Germany) for 1.5–2 h to stabilize the temperature of the ink. The cartridge and the printing bed temperature were set at 26°C and 10°C, respectively. Computer-aided design (CAD) models were designed using Fusion360 (Autodesk, Inc., San Rafael, CA, United States) and sliced using Perfactory RP (Envisiontec GmbH). Squares of 20 × 20 mm were designed, with a distance between fibers of 0.5 mm. The angle between layers was set at 0/90 degrees, and a stainless-steel dispensing tip G23 12.7 mm (Nordson, Duluth, GA, United States) length was used.

Four different GelMA-NPs hydrogels were 3D printed in sterile conditions, i.e., (i) GelMA-C-NPs, (ii) GelMA-Rif-NPs, (iii) GelMA-Van-NPs, and (iv) GelMA-Rif-Van-NPs, a combination of GelMA-Rif-NPs and GelMA-Van-NPs inks in alternated layers (Figure 1d, Table 3). Four-layer hydrogels were printed for all groups. The 3D-printed hydrogels were UV-crosslinked with 25 mW/cm^2 UV light 365 nm (BlueWave 75 UV Light Curing Spot Lamp, Torrington, CT, United States) for 90 s.

2.10. Bacterial strains

S. aureus RN4220[39], *S. aureus* RN4220 Rif-resistant (*S. aureus* RN4220 Rif^R), *S. aureus* RN4220 Van-resistant (*S. aureus* RN4220 Van^R), and *S. aureus* AMC 201[40,41] were used for this study. *S. aureus* RN4220 Rif^R and *S. aureus* RN4220 Van^R were selected by exposing *S. aureus* RN4220 to increasing concentrations of Rif and Van, respectively, for 25 passages (see section 2.11). Prior to experiments, bacteria from frozen stocks were grown overnight at 37°C on sheep blood agar plates (BioMerieux, Marcy l'Etoile, France). For each experiment, fresh subcultures were made in tryptic soy broth (TSB; Oxoid, Hampshire, UK) at 37°C.

2.11. Development of antibiotic resistance in *S. aureus* RN4220

S. aureus RN4220 was cultured overnight at 37°C at 200 rpm in TSB. Then, 100 µL of the overnight culture was transferred to 5 mL TSB and this suspension was incubated for 3 h at 37°C at 120 rpm to reach the exponential growth phase. In wells of a 96-well flat-bottom plate (Greiner bio-one, Monroe, NC, United States), serial dilutions from 128 µg/mL to 0.125 µg/mL of the antibiotics (Rif or Van) in 90 µL were added to 10 µL of bacterial inoculum (final concentration of 10^6 colony forming units (CFU) /mL) and incubated overnight at 37°C and 120 rpm. All incubations were done in duplicates.

The minimum inhibitory concentration (MIC), i.e., the lowest concentration of antibiotic that prevents visible bacterial growth, was determined for each antibiotic. To continue challenging the bacteria with each antibiotic, 2 µL of the well with the highest antibiotic concentration which had allowed visible growth (i.e., ½ MIC) was added to a new plate with serial dilutions of the antibiotics as described above. This was repeated for 25 passages.

The antimicrobial resistant strains were tested for antibiotic susceptibility by VITEK analysis (VITEK, BioMerieux, Marcy l'Etoile, France) to confirm the resistance to each antibiotic.

2.12. Assessment of antibiotic resistance stability

To assess the stability of the antimicrobial resistance, the bacteria were cultured on blood agar plates without antibiotics for 6 passages. Then, an MIC assay combined with a minimum bactericidal concentration (MBC; the concentration that kills ≥99.9% of the bacteria after 24 h) assay was performed for each bacterial strain for each specific antibiotic at each passage. To assess the MBC, duplicate 10 µL aliquots from the 10-fold serial diluted antibiotic suspensions were cultured on blood agar plates at 37°C.

2.13. Kirby–Bauer agar diffusion assay

A Kirby–Bauer agar diffusion assay was performed to determine the zone of inhibition (ZOI) for the different *S. aureus* strains with the GelMA hydrogels containing either C-NPs, Rif-NPs, Van-NPs, or hydrogels of GelMA with Rif-NPs and GelMA with Van-NPs.

First, a bacterial suspension of each strain was prepared by suspending 5 colonies in 5 mL of PBS. Then, Mueller Hinton agar plates (Oxoid) were inoculated with a swab soaked in the bacterial suspension. The hydrogels were placed on the agar plate and incubated overnight at 37°C. The next day, the ZOIs (in mm) were measured at 4 positions, at the middle of each side of the square hydrogel. To assess the antimicrobial activity over time, the procedure was repeated daily for 10 days, by transferring the hydrogels after each incubation to freshly inoculated agar plates.

2.14. In vitro bacterial adhesion assay

An *in vitro* bacterial adhesion assay was performed to assess the antimicrobial activity of the hydrogels and to quantify the number of adhered bacteria. The *S. aureus* strains were cultured to the mid-logarithmic growth phase in TSB at 37°C and 120 rpm, and subsequently diluted in TSB to 1 × 10^6 CFU/mL. Of each bacterial strain, 1 mL of the suspension was added to separate GelMA hydrogels (n= 6 per type of hydrogel) in 24-well plates and incubated overnight at 37°C and 120 rpm. The suspensions were collected in separate tubes for bacterial quantification, and the hydrogels were gently washed twice with demineralized water, subsequently placed in 1.5-mL Eppendorf tubes with

500 µL of PBS, vortexed for 30 s and sonicated at 35 kHz for 15 min in a water bath sonicator (Elma Transsonic T460, Elma) to dislodge adherent bacteria. The suspensions and sonicates were serially diluted and the numbers of viable bacteria were determined by quantitative culture on blood agar plates. An MIC/MBC assay was performed, as described in section 2.12, to determine if the bacteria retrieved from the suspension and detached from the hydrogels had developed resistance.

2.15. Detection of mutation on the rpoB gene

Genomic DNA from selected *S. aureus* Rif-resistant isolates was extracted and used as a template for amplification to assess the presence of mutation(s) in the *rpoB* gene that could explain the resistance. The Rif-resistant *S. aureus* isolates were: *S. aureus* RN4220, *S. aureus* AMC 201, *S. aureus* Rif^R, *S. aureus* RN4220 after contact with GelMA-C-NPs hydrogel, *S. aureus* RN4220 after contact with GelMA-Rif-NPs hydrogel, *S. aureus* AMC 201 after contact with GelMA-C-NPs, and *S. aureus* AMC 201 after contact with GelMA-Rif-NPs hydrogel. A Wizard kit was used for the genomic DNA extraction (Promega, Madison, WI, USA). A 702-bp fragment from nucleotide positions 441–673 corresponding to the Rif resistance-determining region of the *rpoB* gene was amplified with *rpoB* forward (5′-AGTCTATCACACCTCAACAA-3′; Tm 50°C) and reverse (5′-TAATAGCCGCACCAGAATCA-3′; Tm 53°C, 1°C) primers[42] using the high-fidelity Phusion polymerase kit (Invitrogen, Waltham, MA, USA) and an annealing temperature of 50°C. The amplified fragments were purified from agarose gels with the GeneJET Purification kit (Thermo Fisher) and sequenced with the *rpoB* forward and reverse primers at the Core Genomic Facility of the Amsterdam UMC, Amsterdam, the Netherlands. The nucleotide sequences obtained were aligned to the *S. aureus* RN4220 sequence obtained from NCBI (NZ_CP076105.1) by using Benchling.

2.16. Biofilm imaging

SEM was performed to visually confirm the bacterial attachment and biofilm formation on and in the 3D-printed hydrogels. The setup was the same as in section 2.14 until the two washing steps with demineralized water. Before SEM, hydrogels were fixed in 4% (v/v) paraformaldehyde and 1% (v/v) glutaraldehyde (Merck, Kenilworth, NJ, United States) overnight at room temperature. The hydrogels were then rinsed twice with distilled water for 10 min and dehydrated in a graded ethanol concentration series from 50% to 100% of ethanol. The hydrogels were immersed in hexamethyldisilazane (Polysciences Inc., Warrington, FL, United States) overnight and air-dried to reduce the surface tension. Before imaging, the hydrogels were mounted on aluminum SEM stubs and sputter-coated with a 4-nm platinum–palladium layer using a Leica EM ACE600 sputter coater (Microsystems, Wetzlar, Germany). Images were acquired at 3 kV using a Zeiss Sigma 300 SEM (Zeiss, Oberkochen, Germany) at the Electron Microscopy Center Amsterdam (Amsterdam UMC, Amsterdam, the Netherlands). Of each hydrogel, six fields were viewed and photographed at magnifications of 1,000×.

2.17. Statistical analysis

All statistical analyses were performed with GraphPad Prism 9. The statistical analysis for the adhesion assay was performed with a Dunn's multiple comparison test to evaluate the differences between the groups compared to the control group. For all tests, *P*-values of ≤0.05 were considered significant.

2.18. 3D modeling software

3D concepts of hydrogels dual antibiotic-loaded NPs were designed and rendered in 3ds Max (Autodesk Inc.) (Figure 4f–i). BioRender was used to make some of the figures in this article.

3. Results

3.1. PLGA NPs characterization

Non-loaded control PLGA NPs (C-NPs), Rif-NPs and Van-NPs were successfully synthesized with three different molecular weight polymers. C-NPs were prepared with LMW PLGA, whereas Rif-NPs and Van-NPs were prepared with LMW, MMW, or HMW PLGA. SEM characterization was performed to analyze the mean size and the shape of the PLGA NPs. Spherical shape was observed in the C-NPs, Van-NPs, and Rif-NPs (Figure 2). A correlation between MW and mean size was observed, since PLGA LMW produced the smallest NPs in both the Van- and Rif-loaded NPs (Table 1). PDI values below 0.2 were considered monodisperse (homogeneous population), while PDI values above 0.2 were considered polydisperse (heterogeneous population). The non-loaded LMW NPs showed a mean size of 228 nm and a PDI of 0.29, which were a significantly higher mean size and a PDI when compared to the Van- or Rif-loaded LMW NPs (Table 1). The mean size of LMW Van-NPs and LMW Rif-NPs were 207 nm and 164 nm, which were significantly lower than control. The PDIs for both Van-NPs and Rif-NPs were 0.09 and 0.17, respectively, indicating a narrow size distribution.

The drug loading of Rif in the NPs was 68.86, 29.80, and 16.60 mg/mg for LMW, MMW, and HMW, respectively, showing an inverse correlation between drug loading and molecular weight of the polymer. For Van-loaded NPs, the drug loading was 59.98, 40.61, and 68.53 mg/mg for LMW, MMW, and HMW, respectively, without a correlation between drug loading and polymer MW.

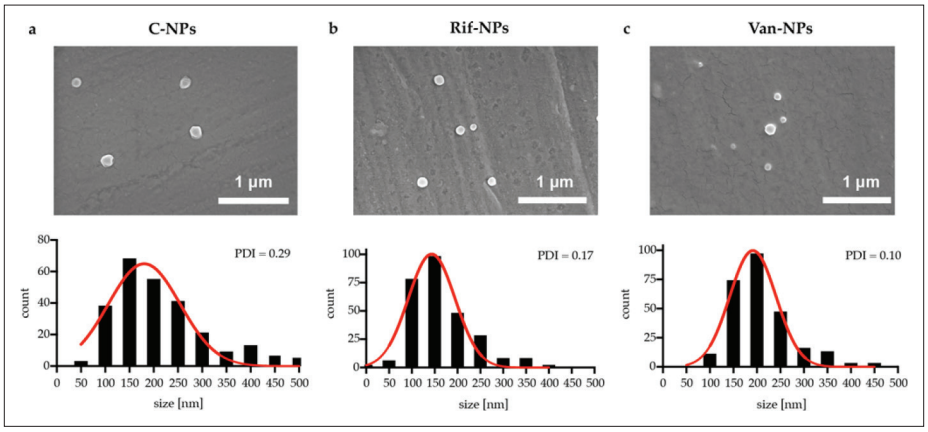

Figure 2. Scanning electron microscopy images and size distribution histograms of (a) non-loaded (control; C-NPs), (b) Rif- and (c) Van-loaded LMW PLGA NPs (n = 250).

Table 1. Mean size ± standard deviation, PDI, encapsulation efficiency, and drug loading of non-loaded (control; C-NPs) and Van- (Van-NPs) or Rif-loaded PLGA NPs (Rif-NPs)

Drug loading	Molecular weight	Mean size (nm)	PDI	Encapsulation efficiency (%)	DL (mg/mg)
Non-loaded (control)	LMW	228 ± 124	0.29		
Rif	LMW	164 ± 67	0.17	21.10	68.86
Rif	MMW	257 ± 83	0.10	20.27	29.80
Rif	HMW	293 ± 76	0.07	12.41	16.60
Van	LMW	207 ± 64	0.10	53.40	59.98
Van	MMW	277 ± 81	0.09	36.60	40.61
Van	HMW	253 ± 78	0.10	60.00	68.53

HMW, high molecular weight; LMH, low molecular weight; MMW, medium molecular weight.

3.2. GelMA and GelMA-PLGA NPs hydrogel characterization

The degree of functionalization (DoF) of GelMA hydrogel was measured by quantifying the amount of the non-reacted amine groups after the chemical modification. The obtained results showed a DoF of 87.9%.

Dynamic shear rheometer analysis was performed to study the physical crosslinking of GelMA and GelMA-C-NPs hydrogels from 5°C to 40°C. This analysis provided quantitative information about the viscoelastic properties of the polymer under periodic rotational strain deformation. The viscosity, the loss modulus (G′), and the storage modulus (G″) were evaluated. The sol–gel temperature increased while the polymer concentration increasing (**Figure S2**), and no significant differences were observed in the sol–gel temperature of GelMA compared to GelMA-C-NPs (Figure 3a and b). The best fiber formation and printability was obtained when the printing-head temperature was set at 27°C (1°C–2°C below the sol–gel temperature).

The compression test showed no significant differences in the Young's modulus of GelMA-C-NPs compared to GelMA without NPs (**Figure S3a** and **b**). An increase in the swelling properties was observed when reducing the GelMA concentration. No differences in swelling properties were observed when loading PLGA NPs into the GelMA hydrogels (**Figure S3c**).

3.3. 3D-printed antimicrobial hydrogels

GelMA-C-NPs, GelMA-Rif-NPs, GelMA-Van-NPs, and GelMA-Rif-Van-NPs were successfully 3D-printed in a total of 4 alternating layers at 0 and 90 degrees, with a 500-µm distance between fibers within each layer (Figure 4a–c). The hydrogels containing the combination of GelMA-Rif-NPs and GelMA-Van-NPs (GelMA-Rif-Van-NPs) were printed with the same printing parameters and intercalating layers of two different inks within four layers (Rif-Van-Rif-Van) (Figure 4c, f–i, Table 2).

3.4. *In vitro* drug release

The cumulative drug release of Rif-NPs and Van-NPs (LMW, MMW, and HMW) is shown in Figure 5. A strong dependency on the molecular weight of the PLGA was observed. For the Rif-NPs with LMW and MMW PLGA and the Van-NPs with LMW PLGA, a biphasic release was observed, with an initial burst release followed by a sustained

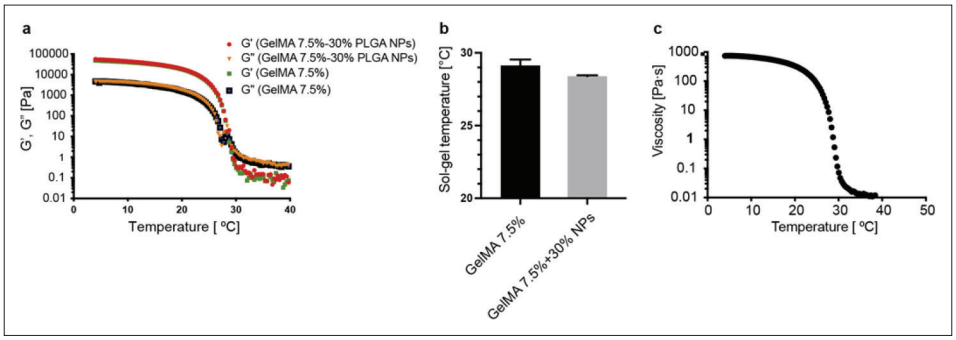

Figure 3. Rheological analysis of GelMA and GelMA-C-NPs. (a) Storage and loss modulus and (b) sol-gel temperatures of GelMA and GelMA-C-NPs, and (c) viscosity of GelMA 7.5 % (w/v) - C-NPs 30 % (w/w).

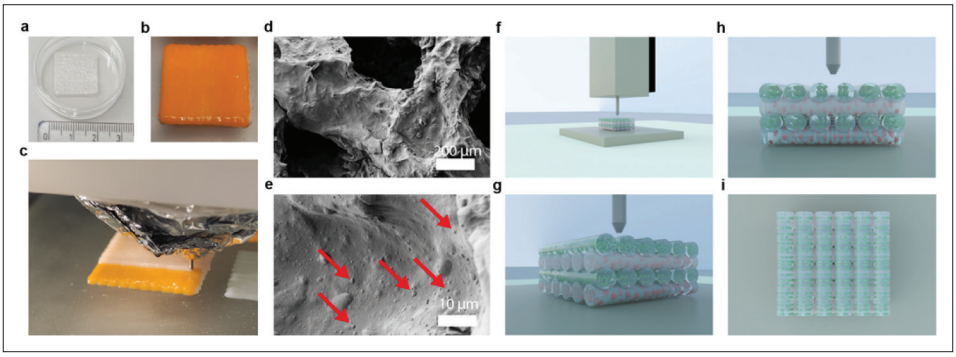

Figure 4. 3D-printed GelMA-PLGA hydrogels with (a) C-NPs and (b) layer-by-layer combination of GelMA with Rif-NPs and Van-NPs. (c) 3D printing process of dual antibiotic GelMA hydrogel (GelMA-Rif-Van-NPs), containing Rif-NPs (orange) and Van-NPs (white) using a 3D bioplotter (Envisiontec). (d, e) SEM images of GelMA-C-NPs (red arrows C-NPs). (f–i) 3D concept of hydrogel-loaded NPs, combining two inks layer by layer.

Table 2. List of 3D-printed GelMA PLGA NPs hydrogels produced for *in vitro* studies

Hydrogel	Nanoparticles	Ink system	Number of layers	Molecular weight of PLGA
GelMA-C-NPs	C-NPs (non-loaded)	Single ink	4 layers	LMW
GelMA-Rif-NPs	Rif-NPs	Single ink	4 layers	LMW
GelMA-Van-NPs	Van-NPs	Single ink	4 layers	LMW
GelMA-Rif-Van-NPs	Rif-NPs and Van-NPs	Double ink, one ink for each NP type	2 + 2 layers alternated	LMW

HMW, high molecular weight; LMH, low molecular weight; MMW, medium molecular weight.

drug release over time. For the Rif-NPs HMW PLGA, a sustained release without a burst release was observed, and the cumulative drug release after 20 days was about 24%. For the Van-NPs with MMW and HMW PLGA, a similar effect was observed without a burst release, and their cumulative drug release was approximately 25% and 3%, respectively, after 20 days. Taken together, the LMW PLGA NPs showed the fastest drug release for the first 3 weeks. LMW PLGA was selected to prepare Rif- and Van-loaded NPs to be incorporated into the 3D-printed GelMA hydrogels.

3.5. Development of antibiotic-resistant *S. aureus* strains

Serial passaging of *S. aureus* RN4220 with sub-inhibitory doses of the antibiotics Rif and Van resulted in the isolation of resistant isolates (Figure 6). The exposure to Rif resulted in a strong increase of the MIC after 10 passages (from 0.0125 to 128 µg/mL). Exposition to Van resulted in an increase of the MIC after 4 passages (from 2 to 16 µg/mL) and a second increase after 23 passages (from 16 to 32 µg/mL).

3.6. Assessment of antibiotic resistance stability

The two *S. aureus* RN4220 Rif^R strains maintained their antibiotic resistance even after 6 passages on blood agar plates without being exposed to Rif. However, the two *S. aureus* RN4220 Van^R strains lost their resistance ability after the first passage in the absence of Van. This reversion of resistance has been previously described for Van *in vitro* and in patients[43]. Therefore, Van was added to the overnight TSB cultures of *S. aureus*

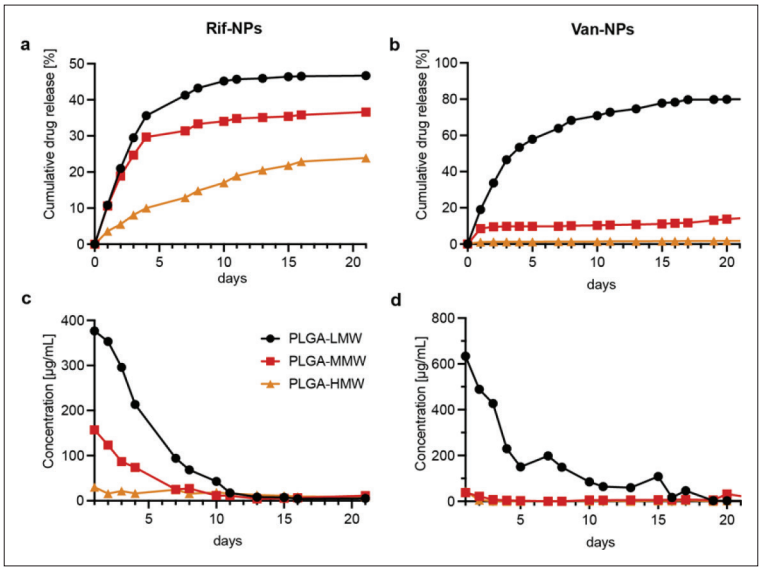

Figure 5. *In vitro* cumulative release and concentration of Rif (a, c) and Van (b, d) from LMW, MMW, and HMW PLGA NPs in PBS at 37°C.

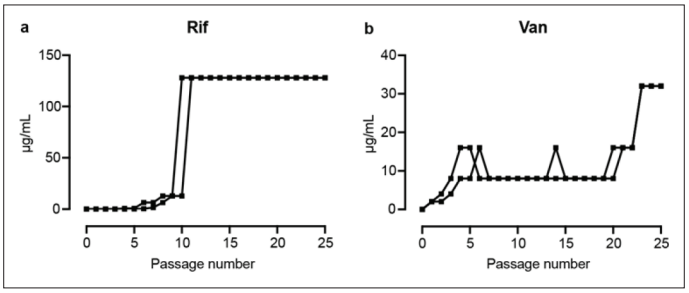

Figure 6. Development of resistance of *S. aureus* RN4220 against Rif (a) and Van (b) over 25 passages (n = 2).

RN4220 Van^R for subsequent experiments to maintain its resistance.

3.7. Antibacterial activity of GelMA-PLGA NPs hydrogels over time

GelMA-Rif-NPs, GelMA-Van-NPs, and GelMA-Rif-Van-NPs hydrogels were transferred to fresh agar plates inoculated with different test strains on a daily basis, and they created a zone of inhibition (ZOI) that prevented bacterial growth for *S. aureus* RN4220 for 10, 9, and 10 days, respectively, with diameters of the zones decreasing over time as expected with the release of the antibiotics (Figure 7a). The GelMA-Van-NPs or GelMA-Rif-Van-NPs showed a ZOI for *S. aureus* RN4220 Rif^R for 7 and 5 days, respectively (Figure 7b). *S. aureus* RN4220 Rif^R showed to be more sensitive for the GelMA-Van-NPs than the other *S. aureus* strains as it showed a larger ZOI. As expected, no ZOI formed around the GelM-Rif-NPs for *S. aureus* RN4220 Rif^R, meaning that the release of Rif did not inhibit the bacterial growth. *S. aureus* RN4220 Van^R showed to be slightly more sensitive to GelMA-Rif-NPs with a ZOI for 10 days and less susceptible to the GelMA-Van-NPs hydrogels with a ZOI for 5 days (Figure 7c). Hence, the high local release of Van was still able to kill Van-resistant bacteria. The clinical *S. aureus* strain AMC 201 had a ZOI with the GelMA-Rif-NPs, GelMA-Van-NPs, or GelMA-Rif-Van-NPs hydrogels for 3, 6, and 3 days, respectively. As expected, GelMA-C-NPs hydrogels did not form any ZOI for any *S. aureus* strain (not shown). In summary, the GelMA-Rif-NPs hydrogels formed ZOI for *S. aureus* RN4220, *S. aureus* RN4220 Van^R, and *S. aureus* AMC201, but not for *S. aureus* RN4220 Rif^R. The GelMA-Van-NPs hydrogels formed ZOI for the four *S. aureus* strains, with *S. aureus* RN4220 Van^R being less susceptible and *S. aureus* RN4220 Rif^R more susceptible than the other strains. The GelMA-Rif-Van-NPs hydrogels formed ZOI for all *S. aureus* strains, showing that this double antibiotic-releasing hydrogel targets both resistant strains.

3.8. Antimicrobial and anti-adhesive activity of the 3D-printed GelMA hydrogels loaded with Rif-NPs and Van-NPs

In vitro antimicrobial and antiadhesive activity of the GelMA-Rif-NPs, GelMA-Van-NPs, or GelMA-Rif-Van-NPs

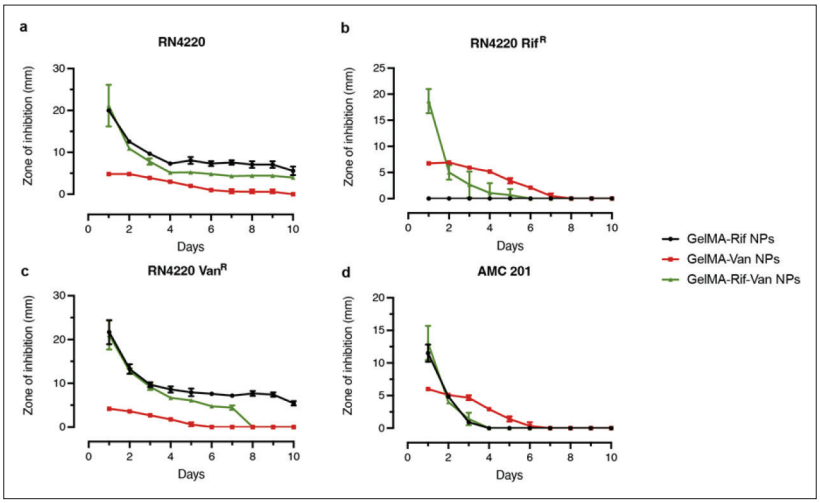

Figure 7. Antimicrobial activity of GelMA-Rif-NPs, GelMA-Van-NPs, or GelMA-Rif-Van-NPs, measured in zone of inhibition (in mm), against *S. aureus* RN4220 (a), *S. aureus* RN4220 Rif^R (b), *S. aureus* RN4220 Van^R (c), and *S. aureus* AMC 201 (d). The hydrogels were tested in the zone of inhibition assays, with a daily transfer of the hydrogels to fresh test plates for 10 days (n = 3).

was assessed using *S. aureus* RN4220, *S. aureus* RN4220 Rif^R, *S. aureus* RN4220 Van^R, and *S. aureus* AMC 201. After incubation of the hydrogels in a suspension of *S. aureus* RN4220 or of *S. aureus* AMC 201 for 24 h, there was a significant reduction in the quantity of adhered bacteria on the hydrogel and planktonic bacteria in the medium of >2-log CFU in the GelMA-Rif-NPs hydrogels. Still, they were not completely eradicated (Figure 8a and e). A MIC assay was performed using the colonies of *S. aureus* RN4220 and *S. aureus* AMC 201 cultured after interacting with the GelMA-C-NPs and GelMA-Rif-NPs hydrogels. Bacteria cultured after incubation with the GelMA-Rif-NPs hydrogels from the supernatant and the hydrogels had a MIC higher than 128 μg/mL, clearly indicating the selection for resistance against Rif. The bacteria from colonies collected after incubation with the GelMA-C-NP hydrogel had a MIC of 0.0019 μg/mL for *S. aureus* RN4220 and 8 μg/mL for *S. aureus* AMC 201, which are identical to those used at the beginning of the experiment, showing that no resistance development had occurred. These results indicate that using biomaterials releasing only Rif has a high risk of resistance development in bacterial species such as *S. aureus*.

A complete eradication of *S. aureus* RN4220 was found with the GelMA-Van-NPs and GelMA-Rif-Van-NPs hydrogels. *S. aureus* RN4220 Rif^R showed a complete prevention of adherence of the bacteria to the hydrogel (Figure 8b) and the planktonic bacteria (Figure 8f) after incubation with the GelMA-Van-NPs or GelMA-Rif-Van-NPs hydrogels. As expected, no reduction was found after incubation of *S. aureus* RN4220 Rif^R with GelMA-Rif-NPs hydrogels due to its resistance to Rif. A complete killing of *S. aureus* RN4220 Van^R after incubation with the GelMA-Rif-NPs or GelMA-Rif-Van-NPs hydrogels was observed (Figure 8c and g). Interestingly, the Van resistance of this strain prevented subsequent resistance development against Rif. Moreover, the number of *S. aureus* RN4220 Van^R colonies was reduced after incubation with GelMA-Van-NPs hydrogels, despite the resistance against Van, suggesting that the released concentrations of Van were higher than the resistance level of this strain.

The GelMA-Van-NPs or GelMA-Rif-Van-NPs hydrogels showed the complete killing of *S. aureus* AMC 201 when these bacteria attached to the hydrogel, as well as of the planktonic cells in suspension (Figure 8d and h). SEM was used to verify the hydrogels' ability to reduce bacterial growth (Figure 8i). Of all *S. aureus* strains, a significant number of bacterial cells were adhered to the GelMA-C-NPs hydrogel surface, forming a biofilm. The GelMA-Rif-NPs hydrogels showed only biofilm formation of the *S. aureus* Rif^R strain. On the GelMA-Van-NPs hydrogels, a few bacterial cells of the *S. aureus* Van^R strain were observed. No bacterial cells were found in the GelMA-Rif-Van-NPs hydrogels (Figure 8). Finally, GelMA-Rif-NPs was partially effective against *S. aureus* RN4220 and *S. aureus* AMC 201 while completely effective against *S. aureus* RN4220 Van^R. GelMA-Rif-NPs did not work against *S. aureus* Rif^R. GelMA-Van-NPs partially worked against *S. aureus* RN4220 Van^R, indicating a high local concentration of Van, which exceeds the resistance level of the strain. The GelMA-Rif-Van-NPs hydrogel killed all *S. aureus* strains tested, including the resistant ones.

Sanger sequencing was used to explain the Rif resistance found after *S. aureus* RN4220 and *S. aureus* AMC 201 were incubated with the GelMA-Rif-NPs. *S. aureus* Rif^R and *S. aureus* RN4220 after incubation with GelMA-Rif-NPs

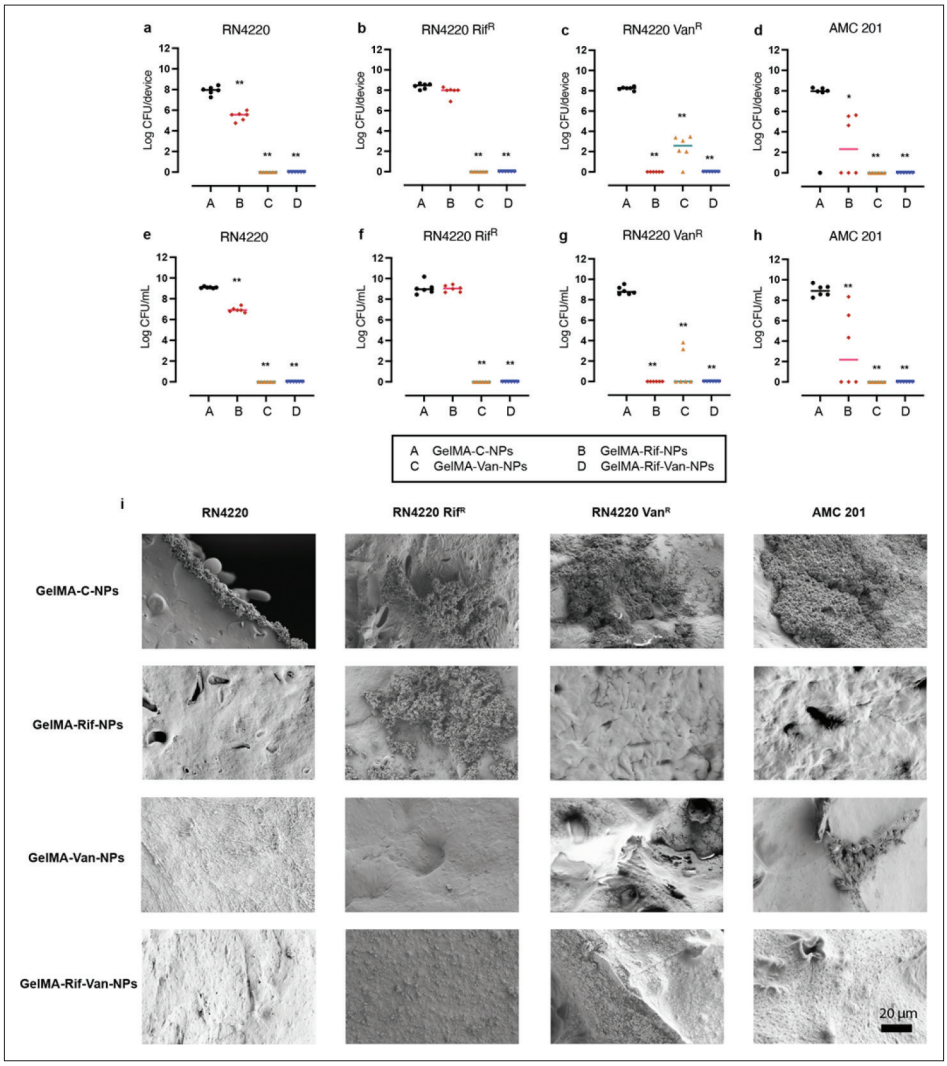

Figure 8. *In vitro* activity of the 3D-printed GelMA-Rif-NPs, GelMA-Van-NPs, and GelMA-Rif-Van-NPs with bacterial attachment (a–d) and planktonic bacterial (e–h) growth in the medium of *S. aureus* RN4220, *S. aureus* Rif^R, *S. aureus* Van^R, and *S. aureus* AMC 201. Each group was analyzed in six replicates and the data are expressed in LogCFU. Note: * indicates a *P*-value of 0.01–0.05, ** indicates a *P*-value of 0.001–0.01. (i) Representative SEM images of each hydrogel inoculated with each bacterial strain at 1,000× magnification.

hydrogels showed three single nucleotide polymorphisms (SNPs) in the *rpoB* fragment that corresponded to three amino acid substitutions, namely S463R (AGC→AGA), D471G (GAC→GGC), and R484H (CGT→CAT) (Table 3). No mutations were found in the *S. aureus* RN4220 cultured with GelMA-C-NPs hydrogel nor in the *S. aureus* AMC 201 isolates cultured from GelMA-C-NPs or GelMA-Rif-NPs. Although *S. aureus* AMC 201 cultured from GelMA-Rif-NPs hydrogel had a high MIC for Rif (>128 µg/mL), no mutations were found in the sequenced amplicon of *rpoB*, indicating another mechanism of resistance.

4. Discussion

Antibiotic-loaded devices are commonly used for local delivery in orthopedics to prevent or treat bone and joint infections. PMMA cement loaded with antibiotics are the most common biomaterials used in clinics and can effectively provide local antimicrobial activity at the surgical site. However, only a limited number of antibiotics can be incorporated in PMMA due to its polymerization at high temperatures. Moreover, their long-term antibiotic release at sub-therapeutic concentration can induce the development of antimicrobial resistance. Using biomaterials like hydrogels can solve both problems, as thermo-labile antibiotics can be incorporated and some hydrogels are biodegradable. The degradation of the polymeric matrix should prevent the release of sub-therapeutic antibiotic concentration[44]. Previous studies have shown the effective incorporation of antibiotics in hydrogels such as an injectable gentamicin-loaded

Table 3. Results of Rif MIC and *rpoB* genotyping

Strain	Rif MIC (μg/mL)	Amino acid position	Nucleotide substitution	Amino acid substitution
S. aureus RN4220	0.0019	No change	No change	No change
S. aureus Rif^R	≥ 128	463 471 484	AGC→AGA GAC→GGC CGT→CAT	S463R D471G R484H
S. aureus RN4220 after contact with GelMA-C-NPs	0.0019	No change	No change	No change
S. aureus RN4220 after contact with GelMA-Rif-NPs	≥ 128	463 471 484	AGC→AGA GAC→GGC CGT→CAT	S463R D471G R484H
S. aureus AMC 201	8	No change	No change	No change
S. aureus AMC 201 after contact with GelMA-Rif-NPs	≥ 128	No change	No change	No change
S. aureus AMC 201 after contact with GelMA-C-NPs	8	No change	No change	No change

Changes compared to *rpoB* sequence of the NCBI Reference Sequence of *S. aureus* RN4220 (NZ_CP076105.1) are indicated.

hyaluronic acid hydrogel that prevented infection in a bone fracture-related infection rabbit model[45], or the coating of a prosthesis with tobramycin- and Van-loaded HA-PLA-PEG hydrogels[46]. In view of the fast diffusion of compounds from hydrogels, providing a sustained release of antibiotics from hydrogels could be challenging. Therefore, in this work, we incorporated Rif-NPs and Van-NPs within a hydrogel to obtain a sustained drug release.

Moreover, some antibiotics are not soluble in water, so new approaches are needed to incorporate such hydrophobic drugs in the hydrogels. In this work, we included Van (hydrophilic) and Rif (hydrophobic) in PLGA NPs using two different techniques: (i) the single (for hydrophobic drugs) and (ii) the double (for hydrophilic drugs) emulsion and evaporation process. The drug release from PLGA NPs using different molecular weights was studied. A correlation between the molecular weight and the release rate was observed for Rif-NPs and Van-NPs, showing that the low molecular weight had the highest release rate after 7 days. These results are aligned with previous studies. Makino *et al.* showed that the release rate of Rif from PLGA microparticles was highly correlated to the molecular weight[47]. Ozalp *et al.* obtained similar results in their study, where they analyzed the release of Van from PLGA NPs using different molecular weights[48]. They observed that the lowest molecular weight PLGA showed the highest release rate of Van. Regarding the endcap group of PLGA, an acid endcap was reported to show a significant faster release than an ester endcap, as the acid endcap group promotes the autocatalytic hydrolysis of the polymer, and hence, a faster degradation and release of the drug. All the PLGA polymers studied in this work were acid endcap[49].

3D-printed antibiotic-loaded hydrogels can be designed and applied for tissue engineering applications or coatings of medical implants for the prevention or treatment of bacterial infections. Combining antibiotics for prevention or treatment of antimicrobial infections may be chosen for incorporation into the hydrogels to be printed before implantation. In this study, we designed and developed 3D-printed gelatin-methacrylate (GelMA) hydrogels carrying PLGA NPs loaded with Van, Rif, or a combination of both. This technology enables the design and manufacturing of a personalized antimicrobial application with a gradual and controlled antibiotic release system to prevent or treat bacterial infections. The antimicrobial activity was evaluated *in vitro* against *S. aureus* strain RN4220 and RN4220 Rif- and RN4220 Van-resistant isolates of this strain and against the clinical *S. aureus* strain AMC 201. The results showed the complete eradication of bacteria by the 3D-printed hydrogel with the dual antibiotic-release NPs. The combination of two antibiotics, such as Rif and Van, in PLGA NPs loaded in the GelMA hydrogel provided sufficient protection against different *S. aureus* strains, including the single antibiotic-resistant *S. aureus* strains. Importantly, contact of *S. aureus* RN4220 with the GelMA-Rif-NPs alone induced the development of resistance against Rif, showing the danger of using Rif alone. Interestingly, although Rif resistance was easily selected if the non-resistant *S. aureus* RN4220 were incubated with hydrogels releasing only Rif, the selection of Rif resistance did not easily occur when *S. aureus* RN4220 resistant to Van were used. The resistance to Van prevented *S. aureus* to easily develop resistance to Rif. This is an important notion since it means that the combination with Van enables Rif to kill *S. aureus* even when these have developed resistance to Van.

Rif acts by interacting with the b-subunit of the bacterial RNA polymerase encoded by the *rpoB* gene. Rif resistance is acquired through key amino acid substitutions in the b-subunit leading to a reduced affinity to the antibiotic[50,51]. In our case, the *rpoB* gene from our *S. aureus* RN4220 Rif resistant isolates cultured from the Rif hydrogels had three SNPs known to cause resistance to Rif[42]. On the other hand, *S. aureus* AMC 201 isolate exposed to GelMA-Rif-NPs hydrogel showed resistance to Rif but did not have any mutation in the *rpoB* gene region studied. To the best of our knowledge, there have been no other resistance mechanisms to Rif reported for *S. aureus*[52,53]. However, referring to the mechanism of resistance development to other antibiotics such as ciprofloxacin, this could be due to an increased expression of efflux pumps[10].

5. Conclusions

The double antibiotic-loaded GelMA hydrogels (GelMA-Rif-Van-NPs) show promising *in vitro* outcomes as an antimicrobial drug delivery system to prevent or treat implant-related infections. In this work, we showed that 3D-printed GelMA hydrogels containing antibiotic-loaded PLGA NPs allows for the design of a combined, controlled, and gradual release system for two antibiotics, which can be used to prevent the development of antimicrobial resistance. In the future, depending on the needs of the patient, this system may be modified to accommodate various implant types, geometries, and antibiotics.

Acknowledgments

We would like to thank Dr. Nehar Celikkin for her technical support in synthesizing gelatin methacrylate and the 3D printing process. We would like to thank Mariusz Nyc for technical support in rheological analysis. We would like to thank Stefany Alonso for her technical support in development of models in 3ds Max Autodesk. We would also like to thank Dr. Nicole van der Wel (Electron Microscopy Center Amsterdam [EMCA], Amsterdam UMC) for her technical assistance in collecting the SEM images. We would like to thank the Core Genomic Facility of the Amsterdam UMC, Amsterdam, the Netherlands for their technical support with sanger sequencing. Benchling Biology Software (2022) was retrieved from https://benchling.com.

Funding

This work was funded by the research project PRINT-AID within the EU Framework Programme for Research and Innovation Horizon 2020 – Marie Skłodowska-Curie Innovative Training Networks under grant agreement No. 722467 and by the National Centre for Research and Development under the grant no. TECHMATSTRATEG2/407770/2/NCBR/2020 entitled New functional MATerials for 3D printing in UROlogy needs, acronym MATURO 3D.

Conflict of interest

The authors declare no conflicts of interest.

Author contributions

Conceptualization: David Martínez-Pérez, Clara Guarch-Pérez, Martijn Riool, Sebastian A. J. Zaat, Wojciech Święszkowski

Funding acquisition: Sebastian A. J. Zaat, Wojciech Święszkowski

Investigation: David Martínez-Pérez, Clara Guarch-Pérez, Muhammad Abiyyu Kenichi Purbayanto

Project administration: David Martínez-Pérez, Clara Guarch-Pérez

Resources: Sebastian A. J. Zaat, Wojciech Święszkowski

Supervision: Emilia Choińska, Martijn Riool, Sebastian A. J. Zaat, Wojciech Święszkowski

Visualization: David Martínez-Pérez, Clara Guarch-Pérez

Writing – original draft: David Martínez-Pérez, Clara Guarch-Pérez

Writing – review & editing: Martijn Riool, Sebastian A. J. Zaat, Wojciech Święszkowski

All authors have read and agreed to the published version of the manuscript.

Ethics approval and consent to participate

Not applicable.

Consent for publication

Not applicable.

Availability of data

Data can be requested from David.perez@pw.edu.pl .

Further disclosure

Some preliminary results were presented at European Society for Biomaterials 2018 and Biofabrication 2018.

References

1. ter Boo G-JA, Grijpma DW, Moriarty TF, *et al.*, 2015, Antimicrobial delivery systems for local infection prophylaxis in orthopedic- and trauma surgery. *Biomaterials*, 52:113–125.

   https://doi.org/10.1016/j.biomaterials.2015.02.020

2. Masters EA, Trombetta RP, de Mesy Bentley KL, *et al.*, 2019, Evolving concepts in bone infection: Redefining "biofilm,"

"acute vs. chronic osteomyelitis," "the Immune Proteome" and "local antibiotic therapy." *Bone Res*, 7(1):20.

https://doi.org/10.1038/s41413-019-0061-z

3. Kavanagh N, Ryan EJ, Widaa A, *et al.*, 2018, *Staphylococcal* osteomyelitis: Disease progression, treatment challenges, and future directions. *Clin Microbiol Reviews*, 31(2):e00084-17, /cmr/31/2/e00084-17.atom.

https://doi.org/10.1128/CMR.00084-17

4. Zimmerli W, Trampuz A, 2011, Implant-associated infection, in *Biofilm Infections*, Bjarnsholt T, Jensen PØ, Moser C, *et al.*, Eds., Springer New York, New York, NY, 69–90.

https://doi.org/10.1007/978-1-4419-6084-9_5

5. Riool M, de Boer L, Jaspers V, *et al.*, 2014, *Staphylococcus epidermidis* originating from titanium implants infects surrounding tissue and immune cells. *Acta Biomater*, 10(12):5202–5212.

https://doi.org/10.1016/j.actbio.2014.08.012

6. Morgenstern M, Vallejo A, McNally MA, *et al.*, 2018, The effect of local antibiotic prophylaxis when treating open limb fractures: A systematic review and meta-analysis. *Bone Joint Res*, 7(7):447–456.

https://doi.org/10.1302/2046-3758.77.BJR-2018-0043.R1

7. Turgut H, Sacar S, Kaleli I, *et al.*, 2005, Systemic and local antibiotic prophylaxis in the prevention of *Staphylococcus epidermidis* graft infection. *BMC Infect Dis*, 5(1):91.

https://doi.org/10.1186/1471-2334-5-91

8. Hendriks JGE, Neut D, van Horn JR, *et al.*, 2005, Bacterial survival in the interfacial gap in gentamicin-loaded acrylic bone cements. *J Bone Joint Surg Br Vol*, 87-B(2):272–276.

https://doi.org/10.1302/0301-620X.87B2.14781

9. Achermann Y, Eigenmann K, Ledergerber B, *et al.*, 2013, Factors associated with rifampin resistance in *Staphylococcal* periprosthetic joint infections (PJI): A matched case–control study. *Infection*, 41(2):431–437.

https://doi.org/10.1007/s15010-012-0325-7

10. Papkou A, Hedge J, Kapel N, *et al.*, 2020, Efflux pump activity potentiates the evolution of antibiotic resistance across *S. aureus* isolates. *Nat Commun*, 11(1):3970.

https://doi.org/10.1038/s41467-020-17735-y

11. Zimmerli W, Sendi P, 2019, Role of rifampin against *Staphylococcal* biofilm infections *in vitro*, in animal models, and in orthopedic-device-related infections. *Antimicrob Agents Chemother*, 63(2):e01746-18.

https://doi.org/10.1128/AAC.01746-18

12. Beeching NJ, Thomas MG, Roberts S, *et al.*, 1986, Comparative *in-vitro* activity of antibiotics incorporated in acrylic bone cement. *J Antimicrob Chemother*, 17(2):173–184.

https://doi.org/10.1093/jac/17.2.173

13. Darouiche RO, Mansouri MD, Zakarevicz D, *et al.*, 2007, In vivo efficacy of antimicrobial-coated devices. *J Bone Joint Surg*, 89(4):792–797.

https://doi.org/10.2106/JBJS.F.00414

14. Inzana J, Trombetta R, Schwarz E, *et al.*, 2015, 3D printed bioceramics for dual antibiotic delivery to treat implant-associated bone infection. *eCM*, 30:232–247.

https://doi.org/10.22203/eCM.v030a16

15. Sanz-Ruiz P, Carbó-Laso E, Del Real-Romero JC, *et al.*, 2017, Microencapsulation of rifampicin: A technique to preserve the mechanical properties of bone cement: Rifampicin-loaded polymethylmethacrylate. *J Orthop Res*, 36(1):459–466

https://doi.org/10.1002/jor.23614

16. Zadpoor AA, Malda J, 2017, Additive manufacturing of biomaterials, tissues, and organs. *Ann Biomed Eng*, 45(1):1–11.

https://doi.org/10.1007/s10439-016-1719-y

17. Alexander AE, Wake N, Chepelev L, *et al.*, 2021, A guideline for 3D printing terminology in biomedical research utilizing ISO/ASTM standards. *3D Print Med*, 7(1):8.

https://doi.org/10.1186/s41205-021-00098-5

18. Ziaee M, Crane NB, 2019, Binder jetting: A review of process, materials, and methods. *Addit Manufac*, 28:781–801.

https://doi.org/10.1016/j.addma.2019.05.031

19. Basit AW, Gaisford S, Eds, 2018, 3D printing of pharmaceuticals, in *AAPS Advances in the Pharmaceutical Sciences Series*, vol. 31, Springer International Publishing, Cham

https://doi.org/10.1007/978-3-319-90755-0.

20. Murr LE, Gaytan SM, Ramirez DA, *et al.*, 2012, Metal fabrication by additive manufacturing using laser and electron beam melting technologies. *J Mater Sci Technol*, 28(1):1–14.

https://doi.org/10.1016/S1005-0302(12)60016-4

21. Jiang T, Munguia-Lopez JG, Flores-Torres S, *et al.*, 2019, Extrusion bioprinting of soft materials: An emerging technique for biological model fabrication. *Appl Phys Rev*, 6(1):011310.

https://doi.org/10.1063/1.5059393

22. Zhuang P, Ng WL, An J, *et al.*, 2019, Layer-by-layer ultraviolet assisted extrusion-based (UAE) bioprinting of hydrogel constructs with high aspect ratio for soft tissue engineering applications. *PLoS One*, 14(6):e0216776.

https://doi.org/10.1371/journal.pone.0216776

23. Li X, Liu B, Pei B, *et al.*, 2020, Inkjet bioprinting of biomaterials. *Chem Rev*, 120(19):10793–10833.

https://doi.org/10.1021/acs.chemrev.0c00008

24. Ng WL, Huang X, Shkolnikov V, *et al.*, 2021, Controlling droplet impact velocity and droplet volume: Key factors to

achieving high cell viability in sub-nanoliter droplet-based bioprinting. *Int J Bioprint*, 8(1):424.

https://doi.org/10.18063/ijb.v8i1.424

25. Sing SL, An J, Yeong WY, *et al.*, 2016, Laser and electron-beam powder-bed additive manufacturing of metallic implants: A review on processes, materials and designs: Laser and electron-beam additive manufacturing of metallic implants. *J Orthop Res*, 34(3):369–385.

https://doi.org/10.1002/jor.23075

26. Dermeik B, Travitzky N, 2020, Laminated object manufacturing of ceramic-based materials. *Adv Eng Mater*, 22(9):2000256.

https://doi.org/10.1002/adem.202000256

27. Li W, Mille LS, Robledo JA, *et al.*, 2020, Recent advances in formulating and processing biomaterial inks for vat polymerization-based 3D printing. *Adv Healthcare Mater*, 9(15):2000156.

https://doi.org/10.1002/adhm.202000156

28. Ng WL, Lee JM, Zhou M, *et al.*, 2020, Vat polymerization-based bioprinting—Process, materials, applications and regulatory challenges. *Biofabrication*, 12(2):022001.

https://doi.org/10.1088/1758-5090/ab6034

29. Slaughter BV, Khurshid SS, Fisher OZ, *et al.*, 2009, Hydrogels in regenerative medicine. *Adv Mater*, 21(32–33):3307–3329.

https://doi.org/10.1002/adma.200802106

30. Bohara S, Suthakorn J, 2022, Surface coating of orthopedic implant to enhance the osseointegration and reduction of bacterial colonization: A review. *Biomater Res*, 26(1):26.

https://doi.org/10.1186/s40824-022-00269-3

31. Liu M, Zeng X, Ma C, *et al.*, 2017, Injectable hydrogels for cartilage and bone tissue engineering. *Bone Res*, 5(1):17014.

https://doi.org/10.1038/boneres.2017.14

32. Ottenbrite, R. M., Park, K., Okano, T., Eds.;, 2010, *Biomedical Applications of Hydrogels Handbook*, Springer New York, New York, NY.

https://doi.org/10.1007/978-1-4419-5919-5

33. Celikkin N, Mastrogiacomo S, Jaroszewicz J, *et al.*, 2018, Gelatin methacrylate scaffold for bone tissue engineering: The influence of polymer concentration: Gelatin methacrylate scaffold for bone tissue engineering. *J Biomed Mater Res*, 106(1):201–209.

https://doi.org/10.1002/jbm.a.36226

34. Wang Y, Qin B, Xia G, 2021, FDA's poly (lactic-co-glycolic acid) research program and regulatory outcomes. *AAPS J*, 23(4).

https://doi.org/10.1208/s12248-021-00611-y

35. Anjum A, Chung P-Y, Ng S-F, 2019, PLGA/xylitol nanoparticles enhance antibiofilm activity *via* penetration into biofilm extracellular polymeric substances. *RSC Adv*, 9(25):14198–14208.

https://doi.org/10.1039/C9RA00125E

36. Toti US, 2011, Targeted delivery of antibiotics to intracellular chlamydial infections using PLGA nanoparticles. *Biomaterials*, 32(27):6606–6613.

https://doi.org/10.1016/j.biomaterials.2011.05.038

37. Khalil NM, Nascimento TCFd, Casa DM, *et al.*, 2013, Pharmacokinetics of curcumin-loaded PLGA and PLGA–PEG blend nanoparticles after oral administration in rats. *Colloids Surf B Biointerfaces*, 101:353–360.

https://doi.org/10.1016/j.colsurfb.2012.06.024

38. Wang H, Zhao Y, Wu Y, *et al.*, 2011, Enhanced anti-tumor efficacy by co-delivery of doxorubicin and paclitaxel with amphiphilic methoxy PEG-PLGA copolymer nanoparticles. *Biomaterials*, 32(32):8281–8290.

https://doi.org/10.1016/j.biomaterials.2011.07.032

39. Rooijakkers SHM, van Wamel WJB, Ruyken M, *et al.*, 2005, Anti-opsonic properties of staphylokinase. *Microbes Infect*, 7(3):476–484.

https://doi.org/10.1016/j.micinf.2004.12.014

40. Kwakman PHS, Velde AAte, Boer L, *et al.*, 2010, How honey kills bacteria. *FASEB J*, 24(7):2576–2582.

https://doi.org/10.1096/fj.09-150789

41. Kwakman PHS, te Velde AA, de Boer L, *et al.*, 2011, Two major medicinal honeys have different mechanisms of bactericidal activity. *PLoS One*, 6(3):e17709.

https://doi.org/10.1371/journal.pone.0017709

42. Aubry-Damon H, Soussy C-J, Courvalin P, 1998, Characterization of mutations in the *RpoB* gene that confer rifampin resistance in *Staphylococcus aureus*. *Antimicrob Agents Chemother*, 42(10):2590–2594.

https://doi.org/10.1128/AAC.42.10.2590

43. Boyle-Vavra S, Berke SK, Lee JC, *et al.*, 2000, Reversion of the glycopeptide resistance phenotype in *Staphylococcus aureus* clinical isolates. *Antimicrob Agents Chemother*, 44(2):272–277.

https://doi.org/10.1128/AAC.44.2.272-277.2000

44. Kang H, Shih Y-RV, Hwang Y, *et al.*, 2014, Mineralized gelatin methacrylate-based matrices induce osteogenic differentiation of human induced pluripotent stem cells. *Acta Biomater*, 10(12):4961–4970.

https://doi.org/10.1016/j.actbio.2014.08.010

45. ter Boo G-JA, Grijpma DW, Moriarty TF, *et al.*, 2015, Antimicrobial delivery systems for local infection prophylaxis in orthopedic- and trauma surgery. *Biomaterials*, 52:113–125.

https://doi.org/10.1016/j.biomaterials.2015.02.020

46. Pitarresi G, Palumbo FS, Calascibetta F, *et al.*, 2013, Medicated hydrogels of hyaluronic acid derivatives for use in orthopedic field. *Int J Pharm*, 449(1–2):84–94.

https://doi.org/10.1016/j.ijpharm.2013.03.059

47. Makino K, Nakajima T, Shikamura M, *et al.*, 2004, Efficient intracellular delivery of rifampicin to alveolar macrophages using rifampicin-loaded PLGA microspheres: Effects of molecular weight and composition of PLGA on release of rifampicin. *Colloids Surf B Biointerfaces*, 36(1):35–42.

https://doi.org/10.1016/j.colsurfb.2004.03.018

48. Özalp Y, Özdemir N, Kocag S, *et al.*, 2001, Controlled release of vancomycin from biodegradable microcapsules. *J Microencapsul*, 18(1):89–110.

https://doi.org/10.1080/026520401750038638

49. Alexis F, 2005, Factors affecting the degradation and drug-release mechanism of poly(lactic acid) and poly[(lactic acid)-co-(glycolic acid)]. *Polym Int*, 54(1):36–46.

https://doi.org/10.1002/pi.1697

50. Wi YM, Greenwood-Quaintance KE, Brinkman CL, *et al.*, 2018, Rifampicin resistance in *Staphylococcus epidermidis*: Molecular characterisation and fitness cost of RpoB mutations. *Int J Antimicrob Agents*, 51(5): 670–677.

https://doi.org/10.1016/j.ijantimicag.2017.12.019

51. O'Neill A, Oliva B, Storey C, *et al.*, 2000, RNA polymerase inhibitors with activity against rifampin-resistant mutants of *Staphylococcus aureus*. *Antimicrob Agents Chemother*, 44(11):3163–3166.

https://doi.org/10.1128/AAC.44.11.3163-3166.2000

52. Williams K, 1998, Accumulation of rifampicin by *Escherichia coli* and *Staphylococcus aureus*. *J Antimicrob Chemother*, 42(5):597–603.

https://doi.org/10.1093/jac/42.5.597

53. Goldstein BP, 2014, Resistance to rifampicin: A review. *J Antibiot*, 67(9):625–630.

https://doi.org/10.1038/ja.2014.107